34th Annual International Conference of the IEEE EMBS
San Diego, California USA, 28 August - 1 September, 2012

# Distal Wall Delineation Using Automated Dual Snake Paradigm: A Multi-Center and Multi-Ethnic Carotid Ultrasound Evaluation

Filippo Molinari, *Member, IEEE,* Kristen M. Meiburger, Luca Saba, Guang Zeng, U. Rajendra Acharya, Mario Piga, Shoaib Shafique, Andrew Nicolaides and Jasjit Suri, *Fellow AIMBE*

*Abstract*— **We present here a novel and patented completely automated IMT measurement system that we developed for common carotid arterial ultrasound longitudinal images, called Carotid Measurement Using Dual Snakes (CMUDS) - a class of AtheroEdge™ system. CMUDS is a dual deformable parametric model (snake) system where the dual snakes evolve simultaneously and are forced to maintain a regularized distance to prevent collapsing or diverging. We benchmarked CMUDS against a conventional single snake (CMUSS). CMUDS is totally automatic while CMUSS is semi-automatic. For performance evaluation, two readers manually traced the lumen-intima (LI) and media-adventitia (MA) borders of our multi-institutional, multi-ethnic, and multi-scanner database of 655 longitudinal B-Mode ultrasound images. CMUDS and CMUSS correctly processed all 665 images. The average IMT biases were equal to 0.030±0.284 mm and -0.004±0.273 mm for CMUDS, and -0.011±0.329 mm and -0.045±0.317 mm for CMUSS. The Figure of Merit of the system was 96.0% and 99.6% for CMUDS and 98.5% and 94.4% for CMUSS. CMUDS improved accuracy (Wilcoxon, $p<0.02$) and reproducibility (Fisher, $p<3\ 10^{-2}$), proving that the novel CMUDS system is adaptable to large multi-centric studies, where a standard IMT measurement technique is required.**

## I. Introduction

A validated predictor of cardiovascular accidents is the intima-media thickness (IMT) of the carotid arteries [1], which is also associated to several cardiovascular diseases (CVDs) [2]. In clinical practice, the sonographer generally manually measures the IMT by placing two caliper markers in correspondence of the lumen-intima (LI) and media-adventitia (MA) interfaces. The distance between the two markers is the estimation of the IMT. Polak *et al.*, however, recently showed that the inter-reader variability in the IMT measurement could cause significant bias in the estimation of the CVD risk of subjects [3].

Touboul *et al.* also discussed the need for standardization in IMT measurement to overcome the limits of manual measurements, showing how a computer system for IMT measurement that ensures high accuracy and reproducibility coupled with high versatility is a clear requirement in multi-center studies [4].

Parametric deformable models (i.e., snakes) are one of the principal typologies of computer methods for carotid far wall segmentation and IMT measurement, because they can accurately follow the regular profile of the wall layers. They are very versatile but can suffer from the need of an initialization (i.e., starting points of the snake algorithm) and from their sensitivity to noise. We developed an innovative Dual Snake paradigm for the automatic tracings of the carotid LI/MA borders and IMT measurement. We called this novel system CMUDS (Carotid Measurement Using Dual Snake). We validated CMUDS on a multi-institutional, multi-ethnic, and multi-scanner database of 665 longitudinal carotid B-Mode images and finally, we benchmarked CMUDS against a traditional snake model as proposed by Loizou *et al.* (called here CMUSS: Carotid Measurement Using Single Snake) [5].

## II. Materials and Methods

### A. CMUDS: Carotid Measurement Using Dual Snakes

Snake-based segmentation techniques must trace the profiles of the LI and MA interfaces. When used as deformable models, snakes are usually initialized close to these interfaces. They must then evolve until their final boundary is correctly aligned with the LI/MA profiles as interpreted by the reader. In our technique, this process is completely automated, meaning that the initialization, evolution, and final convergence do not require any intervention by the user. Our CMUDS system consists of three steps: (1) the automated carotid recognition and tracing of the far adventitia profile ($AD_F$); (2) the initialization of two snake models (one for the LI interface and one for the MA); (3) the convergence and final LI/MA tracing.

#### 1) Step I: Carotid recognition and $AD_F$ wall tracing

For carotid recognition, the $AD_F$ profile was automatically traced by means of a recognition system based on a first-order Gaussian filtering and multi-resolution approach. We named this technique CAMES and it is fully described in the work by Molinari *et al.* [6]. Briefly, it is based on down-sampling the image, speckle reduction, filtering by a first order derivative Gaussian kernel, column-by-column heuristic search for the $AD_F$ point, and final up-sampling to the original image size.

#### 2) Step 2: LI and MA snakes initializations

The $AD_F$ profile was then used to initialize both snakes. The LI snake was initialized by shifting the $AD_F$ profile 3

F. Molinari and K. M. Meiburger are with the Biolab, Department of Electronics and Telecommunications, Politecnico di Torino, 10129 Torino, Italy; (e-mail: filippo.molinari@polito.it).
L. Saba and M. Piga is with the Dept. of Radiology, A.U.O. Cagliari, Cagliari, Italy.
U. R. Acharya is with the Dept ECE, Ngee Ann Polytechnic, Singapore, Singapore.
Shoaib Shafique, MD is with CorVas, West Lafayette, Indiana, USA.
A. Nicolaides, PhD, is with the Vascular Diagostic Center, Nicosia, Cyprus.
J. S. Suri, MS, PhD, MBA is CTO of AtheroPoint LLC, CA, USA and Biomedical Technologies, Inc., CA, USA and is also affiliated Research Professor with Department of Biomedical Engineering, Idaho State University, Pocatello, ID 83201 USA (jsuri@comcast.net).

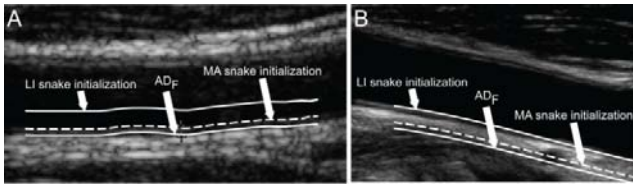


Fig. 1 Automated initialization of the lumen-intima (LI - top white line) and media-adventitia (MA - dashed line) snakes starting from the far adventitia ($AD_F$ - bottom white line) profile.

mm upwards (towards the near wall). Our database showed a maximum IMT value of 1.7 mm, so empirically twice this distance would ensure that the LI snake was placed in the carotid lumen. So we took a round figure of 3 mm for the entire database. The MA snake was initialized by shifting the $AD_F$ profile upwards by 0.1 mm. This value was optimal to place the initial MA snake close to the interface without placing it in between the LI/MA boundaries. Fig. 1 shows the $AD_F$ profile and the snake initializations.

*3) Step 3: CMUDS snake model and its convergence*

A 2-D parametric deformable model (snake) is a mathematical description of a contour evolving on the image and driven by two energy types: internal energies and external energies. Convergence is reached when the internal forces counterbalance the external ones.

Let $v(s)$ represent the snake, a 2D contour, where the parameter *s* is the curvilinear coordinate on the image. The curvilinear coordinate *s* is space-normalized in the range [0,1]. The typical energy functional of a snake $v(s)$ can be expressed as:

$$E\left(v(s)\right)=\int_0^1 \alpha\left|v'(s)\right|^2+\beta e\left(v(s)\right)+\gamma\left|v(s)-e\left(v(s)\right)\right|ds \qquad (1)$$

In eq. (1), the internal energy $E_i$ consists of the first term:

$$E_i\left(v(s)\right)=\int_0^1 \alpha\ \left|v'(s)\right|^2 ds \qquad (2)$$

Whereas the external energy $E_e$ is the second term:

$$E_e\left(v(s)\right)=\int_0^1 \beta\ e\left(v(s)\right)+\gamma\ \left|v(s)-e\left(v(s)\right)\right|ds \qquad (3)$$

The internal energy is used to constrain the shape of the contour and its properties. Specifically, the term $\alpha\ \left|v'(s)\right|^2$ prevents the snake from presenting an excessive curvature. The parameter $\alpha$ is used to control the curvature, whereas $v'(s)$ is the first-order derivative of the snake curve $v(s)$. The square modulus is needed in order to make this term energy.

The external energy is used to attract the snake towards the image discontinuities. The first term of the external energy $\beta\ e\left(v(s)\right)$ is used for capturing the LI/MA interfaces of the far wall. In fact, the functional $e(x,y)$ is an edge operator called FOAM (First Order Absolute Moment), which was

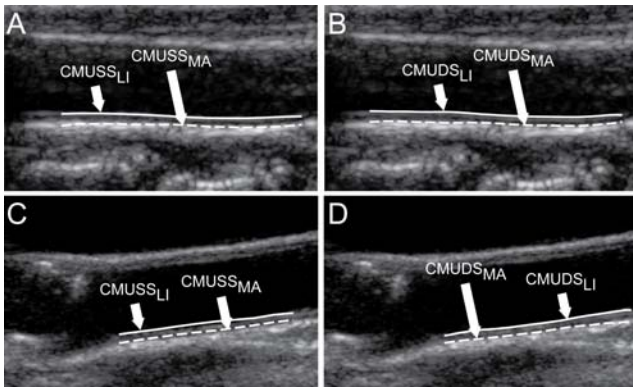


Fig. 2. Samples of CMUSS (left column) and CMUDS LI/MA tracings. Panels A and B are relative to a straight and horizontal artery, and panels C and D to a inclined artery. In these images, CMUSS and CMUDS both showed accurate tracings. $CMUSS_{LI}$ – lumen-intima tracing by CMUSS; $CMUSS_{MA}$ – media-adventitia tracing by CMUSS; $CMUDS_{LI}$ – lumen-intima tracing by CMUDS; $CMUDS_{MA}$ – media-adventitia tracing by CMUDS.

proposed by Demi *et al.* [7] and adapted by Faita *et al.* for detection of the LI/MA edges [8]. This first term of the external energy acts as a stopping function, having a high weight when the snake points are in correspondence to the image edges and blocking the points there. The parameter $\beta$ controls the strength of this stopping force.

The energy term $\beta\ e\left(v(s)\right)$ is null when the snake points are placed far from the edges, where the FOAM operator is equal to zero. Therefore, we added a second term of external energy, $\gamma\ \left|v(s)-e\left(v(s)\right)\right|$, which attracts the snake points when they are far from the edges. This term computes the distance (*i.e.*, the difference) between the edges $e(x,y)$ of the image and the snake position. So, even if the snake is placed where the FOAM is null, it is attracted by the closest edge of FOAM itself, with an attraction force that is proportional to the distance of the snake from the edge. $\gamma$ describes the attraction energy of this second term, which is always positive when the snake is far from the edges, but becomes zero valued when the snake is found in correspondence to the edges. The joint action of the two terms of external energy attracts the snake to the edges and locks the snake once it has reached a stable position.

We used two distinct snakes for the two LI/MA profiles, so there was a total of six parameters: three for the LI snake ($\alpha_{LI}$, $\beta_{LI}$, and $\gamma_{LI}$) and three for the MA snake ($\alpha_{MA}$, $\beta_{MA}$, and $\gamma_{MA}$). Table 1 summarizes these parameter values, which we chose after pilot tests on a subset of 20 images randomly selected from our database (results not reported here). Different parameters for the LI and MA snakes were necessary because, as Faita *et al.* [8] pointed out, the LI and MA edges have different intensities in the FOAM edge map. So initially, the two snakes had the same shape. Then, each snake evolved according to their respective energies. We observed that two possible errors could be presented when

the LI and MA snakes (a) collapse on each other; or (b) diverge more than 3 mm from each other.

To prevent these two potential error conditions, we introduced a mutual constraint that forced the snakes to maintain a constrained distance from one other. At each iteration step of the snake's evolution, we computed the coordinates of both snakes. When the snakes were too close or too far from each other (*i.e.,* the points of the snakes had a mutual distance lower than 0.3 mm or higher than 3 mm, respectively) we shifted those points up or down until the distance was within the imposed constraints. We used the Polyline distance (PDM) as the distance metric [9], because it is almost insensible to the number of points constituting the LI/MA profiles. Finally, we set a maximum limit on the number of iterations (called $I_{MAX}$), which we took equal to 200.

TABLE I – PARAMETERS VALUE FOR THE LI AND MA SNAKES. SUCH VALUES ARE SAME FOR ALL THE IMAGES OF THE DATABASE.

| | $\alpha$ (curvature) | $\beta$ (stopping energy) | $\gamma$ (attraction energy) |
|---|---|---|---|
| LI snake | 0.5 | 0.1 | 0.1 |
| MA snake | 0.5 | 0.2 | 0.05 |

### *B. CMUSS: Carotid Measurement Using a Single Snake*

The single snake method (CMUSS) we adapted was the technique proposed by Loizou *et al.* [5], since it was the most performing and established snake-based technique for LI/MA segmentation and IMT measurement. The first step is based on image pre-processing and snake initialization whereas the second step is the snake-based LI/MA segmentation. Complete details of this algorithm can be found in [5].

### *C. Image database, performance assessment and statistics*

We tested CMUDS and CMUSS on a database of 665 longitudinal B-Mode images, which is multi-institutional, multi-ethnic, multi-scanner, and multi-operator. Each Institution obtained approval for the data acquired by the respective Ethical Committee or Institutional Review Board. The five image datasets were acquired independently from each Institution and in different years. No standardization was made among the five sets, and each sonographer adjusted the scanner settings for each corresponding patient during acquisition. All images were discretized at 8 bits (256 gray levels) and were provided in a digital form. A neurosonographer and an expert vascular radiologist manually segmented all the images by tracing the LI and MA profiles using ImgTracer™ (Global Biomedical Technologies, Inc., CA, USA) [10]. The manual segmentations were considered as ground truth for the system performance evaluation of the computer-generated profiles and IMT measurements. The first reader will be indicated as Reader-1, the second as Reader-2. We used the Wilcoxon signed rank test to assess the difference between the average measurement values, and the Fisher's F-test to test the difference of the variances.

## III. RESULTS

CMUSS and CMUDS both successfully processed the 665 images of the testing database. This is especially important for CMUDS, since it is a completely automated technique. Figure 2 shows samples of CMUSS and CMUDS segmentation. Both techniques showed accurate LIMA tracings despite the different artery anatomy.

CMUSS showed an average IMT value equal to 0.747±0.167 mm, whereas the average CMUDS IMT value was 0.788±0.288 mm. The average values measured by Reader-1 and Reader-2 were 0.758±0.285 mm and 0.791±0.258 mm, respectively.

TABLE 2 – PERFORMANCE EVALUATION COMPARISONS BETWEEN CMUSS (LEFT COLUMN) AND CMUDS (RIGHT COLUMN)

| | **CMUSS** | **CMUDS** |
|---|---|---|
| IMT bias (mm) w.r.t Reader-1 | -0.011±0.329 | 0.030±0.284 |
| IMT bias (mm) w.r.t Reader-2 | -0.045±0.317 | -0.004±0.273 |
| IMT abs. err. (mm) w.r.t Reader-1 | 0.245±0.219 | 0.199±0.205 |
| IMT abs. err. (mm) w.r.t Reader-2 | 0.227±0.226 | 0.180±0.205 |
| FoM (%) w.r.t Reader-1 | 98.5% | 96.0% |
| FoM (%) w.r.t Reader-2 | 94.4% | 99.6% |

Table 2 summarizes the IMT measurement errors and absolute error for CMUSS and CMUDS compared to the readers. The measurement accuracy was high (*i.e.,* the mean value of the IMT bias was low) and the best value was shown by CMUDS when compared to Reader-2 (-0.004 mm, approximately 0.4% of error on the nominal IMT value of 1 mm). The lowest accuracy was shown by CMUSS when compared to Reader-2 (-0.045 mm, about 4.5% of the nominal IMT value). The CMUSS IMT estimates were statistically different from those of Reader-1 ($p<0.04$), but not from those of Reader-2 ($p>0.4$). The CMUDS IMT values, instead, were not different from either of the readers' values ($p>0.2$). The measurement reproducibility was always higher (*i.e.* the standard deviation of the IMT bias was lower) for CMUDS ($p<2.6\ 10^{-4}$ for Reader-1 and $p<1.6\ 10^{-4}$ for Reader-2). Hence, CMUDS measurements were overall more reproducible than CMUSS.

The last two rows of Table 2 reports the Figure of Merit (FoM) [6], which can be thought of as the percent overall agreement between the IMT measurements by the readers and the computer measured IMT. CMUSS showed a FoM equal to 98.5% compared to Reader-1 and of 94.4% to Reader-2. CMUDS demonstrated a FoM of 96.0% compared to Reader-1 and 99.6% to Reader-2. Overall, CMUDS showed the highest FoM (99.6% against Reader-2) and the best average FoM (97.8% against 96.5% of CMUSS).

Figure 3 reports the Bland-Altmann plots for CMUSS (Fig. 3.A and 3.C) and CMUDS (Fig. 3.B and 3.D) with respect to the readers' IMT values.

## IV. DISCUSSION

In this paper we benchmarked our constrained snake model (CMUDS) with the most performing conventional snake model (CMUSS) for the far carotid wall segmentation and IMT measurement. This system is unique and novel in the medical imaging scenario for the following primary reasons: (1) Dual Snake System: two deformable parametric models (one for the LI and one for the MA) are initialized

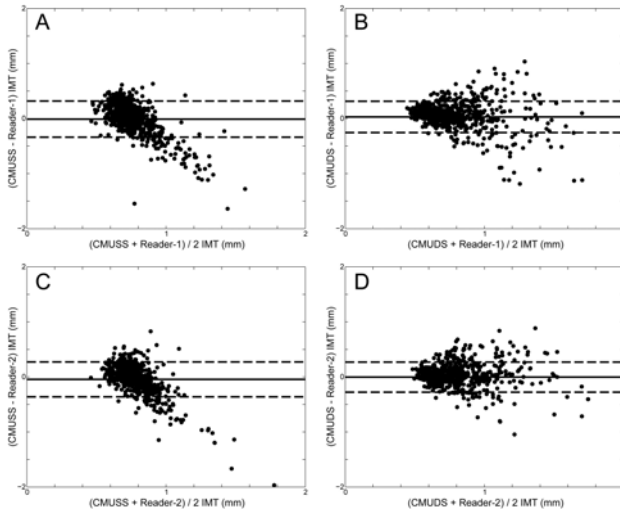


Fig. 3. Bland-Altmann plots for CMUSS (left column) and CMUDS (right column) compared to the readers' IMT values. The top row (panels A and B) is relative to Reader-1, the bottom panels (C and D) to Reader-2.

simultaneously and converge jointly step-by-step; (2) Constrained Paradigm: the LI and MA profiles are constrained during the evolution process; (3) Automation: the entire system, including CCA recognition, ROI estimation, snake initialization, snake evolution and convergence, is completely automated; (4) External Energy: this term utilizes a high-performance edge snapper called FOAM [8] compared to conventional gradient methodologies.

Fig. 3 shows that CMUSS has a marked tendency to underestimation for higher IMT values, while CMUDS showed no bias. Images with high IMT values are relative to high-risk patients, which usually have an irregular ultrasound representation of the wall due to lipid deposits (fig. 4). In such condition, CMUSS profiles could collapse, thus producing an underestimation of the actual IMT (fig. 4.A). In the CMUDS system the LI/MA snakes evolve simultaneously and are constrained by each other, preventing them from diverging or collapsing (fig 4.B).

The best performing snake-based algorithms that have been published in literature were by Cheng *et al.* [11] and Delsanto *et al.* [12]. However, the direct comparison of CMUSS and CMUDS performance with respect to previous snake-based techniques is not straightforward due to the fact that (a) different distance metrics were adopted, (b) our dataset is multi-institutional with varying pixel density, (c) our dataset included both normal and pathological arteries.

## V. Conclusions

We benchmarked CMUDS, a dual-snake constrained snake system for the carotid wall segmentation and IMT measurement against CMUSS, a single snake unconstrained system. We showed that the mutual constraint between the LI and MA snakes in CMUDS increases the overall system performance with greater clinical stability, showing a reproducibility that was statistically better than CMUSS.

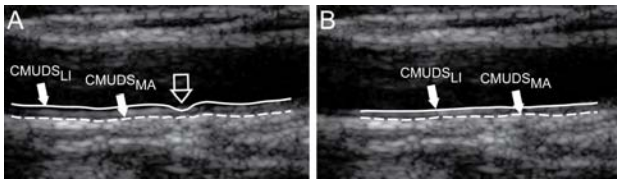


Fig. 4. Comparison between unconstrained (panel A) and constrained CMUDS (panel B). The white arrow indicates a region where the LI snake (continuous white line) collapsed on the MA (dashed white line) due to lack of external energy.

CMUDS is fully automated and had 100% success on a large dataset of 665 images coming from different clinical centers.

The potentialities of CMUDS represent a valuable clinical asset in large epidemiological studies.

## References


[1] I.M. van der Meer, M.L. Bots, A. Hofman, A.I. del Sol, D.A. van der Kuip, and J.C. Witteman, "Predictive value of noninvasive measures of atherosclerosis for incident myocardial infarction: the Rotterdam Study," *Circulation*, vol. 109, (no. 9), pp. 1089-94, Mar 9 2004.

[2] J. Polak, M. Pencina, D. Herrington, and D. O'Leary, "Associations of edge-detected and manual-traced common carotid intima-media thickness measurements with Framingham risk factors: The multi-ethnic study of atherosclerosis," *Stroke*, vol. 42, pp. 1912-1916, 2011.

[3] J. Polak, L. Funk, and D. O'Leary, "Inter-reader differences in common carotid artery intima-media thickness: Implications for cardiovascular risk assessment and vascular age determination," *J. Ultrasound Med.*, vol. 30, pp. 915-920, 2011.

[4] P.J. Touboul, P. Prati, P.Y. Scarabin, V. Adrai, E. Thibout, and P. Ducimetiere, "Use of monitoring software to improve the measurement of carotid wall thickness by B-mode imaging," *J. Hypertens. Suppl.*, vol. 10, (no. 5), pp. S37-41, Jul 1992.

[5] C.P. Loizou, C.S. Pattichis, M. Pantziaris, T. Tyllis, and A. Nicolaides, "Snakes based segmentation of the common carotid artery intima media," *Med. Biol. Eng. Comput.*, vol. 45, (no. 1), pp. 35-49, Jan 2007.

[6] F. Molinari, C. Pattichis, G. Zeng, L. Saba, U. Acharya, R. Sanfilippo, A. Nicolaides, and J. Suri, "Completely Automated Multi-resolution Edge Snapper (CAMES) : A New Technique for an Accurate Carotid Ultrasound IMT Measurement: Clinical Validation and Benchmarking on a Multi-Institutional Database.," *IEEE Trans Image Process*, pp. Sep 23. [Epub ahead of print], 2011.

[7] M. Demi, M. Paterni, and A. Benassi, "The first absolute central moment in low-level image processing," *Computer Vision and Image Understanding*, vol. 80, (no. 1), pp. 57-87, OCT 2000.

[8] F. Faita, V. Gemignani, E. Bianchini, C. Giannarelli, L. Ghiadoni, and M. Demi, "Real-time measurement system for evaluation of the carotid intima-media thickness with a robust edge operator," *J. Ultrasound Med.*, vol. 27, (no. 9), pp. 1353-61, Sep 2008.

[9] J.S. Suri, R.M. Haralick, and F.H. Sheehan, "Greedy algorithm for error correction in automatically produced boundaries from low contrast ventriculograms," *Pattern Anal. Appl.*, vol. 3, (no. 1), pp. 39-60, 2000.

[10] L. Saba, R. Lippo, N. Tallapally, F. Molinari, R. Montisci, G. Mallarini, and J. Suri, "Evaluation of Carotid Wall Thickness by Using Computed Tomography and Semiautomated Ultrasonographic Software," *J. Vasc. Ultrasound*, vol. 35, (no. 3), pp. 136-142, 2011.

[11] D.C. Cheng, A. Schmidt-Trucksass, K.S. Cheng, and H. Burkhardt, "Using snakes to detect the intimal and adventitial layers of the common carotid artery wall in sonographic images," *Comput. Methods Programs Biomed.*, vol. 67, (no. 1), pp. 27-37, Jan 2002.

[12] S. Delsanto, F. Molinari, P. Giustetto, W. Liboni, S. Badalamenti, and J.S. Suri, "Characterization of a Completely User-Independent Algorithm for Carotid Artery Segmentation in 2-D Ultrasound Images," *Instrumentation and Measurement, IEEE Transactions on*, vol. 56, (no. 4), pp. 1265-1274, 2007.